2-μm Wavelength Grating Coupler, Bent Waveguide, and Tunable Microring on Silicon Photonic MPW

Jiayuan Li, Yingjie Liu, Yafei Meng, Ke Xu, *Member, IEEE*, Jiangbing Du, *Member, IEEE*, Fengqiu Wang, Zuyuan He, *Senior Member, IEEE*, and Qinghai Song

***Abstract*— The 2-μm wave band is emerging as a promising spectral window for optical communications and gas sensing. With the increasing demand for components at this wavelength range, developing 2-μm devices is thus required. Silicon photonics is an ideal device technology as it offers several unique advantages of potential low cost and large scale integration. Besides, the silicon nanowire waveguide is transparent and suffers from negligible two photon absorption at 2-μm wavelengths. Here, we report the demonstration of grating coupler, waveguide bend, and thermally tunable microring filter on a multi-project wafer which is fabricated using CMOS compatible process. The peak coupling efficiency of the grating coupler is measured to be −8.4 dB at 1952 nm. The bending losses for the rib waveguide and the strip loaded waveguide are measured with different radii. The ring resonator is fabricated and tested with an underestimated *Q* factor of 1520 (through port) which is due to the limitation of the laser linewidth and wavelength tuning resolution. The extinction ratio exceeds 20 dB and the ring resonance can be thermally tuned by a Titanium Nitride heater. The tuning efficiency is 0.17 nm/mW.**

***Index Terms*— Optical waveguides, waveguide devices.**

I. Introduction

THE two micron spectral band is located between the near infrared and mid infrared spectra, and has unique optical properties like low-loss transmission in silica fiber and significant absorption bands for many gas species [1]. The availability of the laser [2], optical amplifier [3], modulator [4], and the photodetector [5], [6] enables 2-μm optical communications which is under intensive research recently [7]–[11]. Compared with the 1.55-μm band, the components at this waveband are still undeveloped. Among the well-established device technologies, the photonic integration platform is a preferred approach for 2-μm components due to many advantages such as small footprint, large volume, potential low power consumption and so forth [12]. There are several recent demonstrations on integrated functional elements at two micron wavelengths like arrayed waveguide gratings [13] and multimode interferometer [14] on InP substrate. Monolithic waveguide photodetector [15], hybrid integrated photodiode [16] and wavelength multiplexer [17] fabricated on silicon-on-insulator (SOI) have been reported as well. In order to facilitate this band to be of practical use, it is essential to fill in the missing 2-μm devices.

Wavelength selective devices are of general interest due to their wide scope of applications including wavelength division multiplexed data transmission, spectral sensing and spectroscopy. Add-drop waveguide ring resonator is a robust and highly functional wavelength selective device that has been widely used for optical communications [18]–[20], signal processing [21]–[23], optical sensing [24], nonlinear optics [25], quantum optics [26] and so on. The add-drop ring resonator working at 1.3 and 1.5-μm has been included as a library component in the design kit. The ring resonator operating at two micron band can also be a key component since it can function as add-drop filter, optical sensor, spectrometer, frequency discriminator etc. The 2-μm microring fabricated in-lab has been reported recently, but the device only works for fixed wavelengths.

In this work, we for the first time characterize the bending loss for silicon waveguide at 2-μm and demonstrate the grating coupler and tunable microring using silicon photonic multi-project wafer (MPW) shuttle run. The 2-μm and 1.55-μm components are monolithically integrated on the same wafer and share the same fabrication process. The results indicate a reasonable coupling efficiency between optical fiber and the silicon submicron waveguide. The bending losses of both strip and rib waveguide are measured to be consistent with the theoretical predictions. Finally a tunable add-drop microring resonator working at two micron band is achieved. In the following sections, we present the results for grating coupler, waveguide bends and the tunable microring resonator, respectively.

II. Grating Coupler

Several silicon photonic foundries have been providing low-cost photonic integrated circuits (PIC) fabrication for

Manuscript received September 24, 2017; revised January 11, 2018; accepted January 11, 2018. Date of publication February 1, 2018; date of current version February 12, 2018. This work was supported in part by the National Natural Science Foundation of China under Grant 61505039 and Grant 61675128, in part by the Shenzhen Municipal Science and Technology Plan Project under Grant JCYJ20170307151047646, and in part by Open Fund of BUPT under Grant IPOC2016B005. *(Corresponding author: Ke Xu.)*

J. Li, Y. Liu, K. Xu, and Q. Song are with the Department of Electronic and Information Engineering, Harbin Institute of Technology at Shenzhen, Shenzhen 518055, China (e-mail: kxu@hit.edu.cn).

Y. Meng and F. Wang are with the Collaborative Innovation Center of Advanced Microstructures, School of Electronic Science and Engineering, Nanjing University, Nanjing 210008, China.

J. Du and Z. He are with the State Key Laboratory of Advanced Optical Communication Systems and Networks, Shanghai Jiao Tong University, Shanghai 200240, China (e-mail: dujiangbing@sjtu.edu.cn).

Color versions of one or more of the figures in this letter are available online at http://ieeexplore.ieee.org.

Digital Object Identifier 10.1109/LPT.2018.2799194

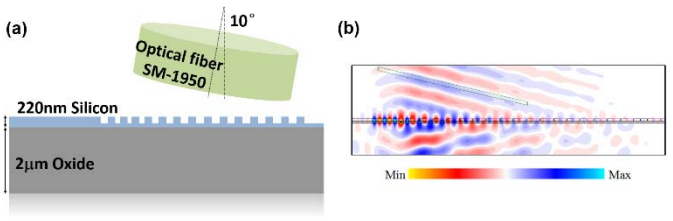

Fig. 1. (a) The side view schematic diagram of the grating coupler which couples the light into SM-1950 fiber. (b) The 2D FDTD simulated optical field of the diffraction.

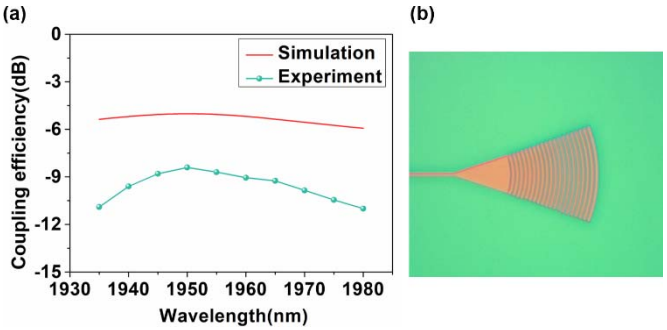

Fig. 2. (a) The simulated coupling efficiency by FDTD and the measured coupling efficiency of the grating coupler. (b) The microscope image of the grating coupler.

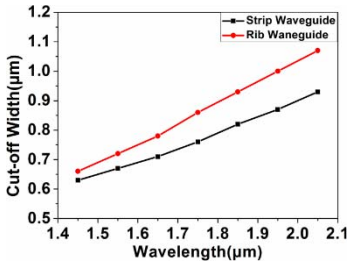

Fig. 3. The maximum waveguide width allowed for single quasi-TE mode.

Fig. 4. The calculated TE mode optical field distribution of the (a) strip waveguide and (b) rib waveguide with 130 nm etching depth.

academic institutions and fabless companies for nearly a decade. The SOI wafer with 220 nm top silicon and 2 μm buried oxide (BOX) has been widely accepted as the substrate for silicon photonics MPW shuttle run. Though the wafer parameters are chosen to optimize the devices at 1.5-μm band, it is highly desirable to design efficient 2-μm components on the same SOI substrate and with the same fabrication process. Thus we first design the two micron grating coupler on SOI with 220 nm top silicon and 2 μm BOX layer. The grating coupler is designed with 10-degree tilt and 130 nm etching depth, as shown in Fig. 1 (a). This etching depth can be realized by the silicon etching process for modulators. The grating structure has an apodized period to match the optical field distribution in SM1950 single mode fiber at two micron band. The gating period (nm) and fill factor are 872 (0.209), 872 (0.209), 872 (0.209), 870 (0.211), 869 (0.216), 866 (0.222), 863 (0.237), 859 (0.26), 859 (0.296), 862 (0.343), 872 (0.395), 889 (0.445), 911 (0.485), 935 (0.504), 955 (0.504), 964 (0.484), 964 (0.452), 955 (0.413), 938 (0.377), 909 (0.354). The SM-1950 fiber has a core diameter of 7 μm and the corresponding mode field diameter of $\sim$8 μm at 1950 nm. The 2D finite difference time domain (FDTD) simulation is performed to design the grating coupler. The diffracted optical field is shown in Fig. 1 (b). We observe a considerable amount of light leaked into the substrate. A main reason is the BOX layer thickness is not large enough since it is the same order as the wavelength. The coupling efficiency is simulated considering the mode overlap between the diffracted field and the mode field in optical fiber. The calculated coupling efficiency is 31% ($-$5 dB) at 1950 nm as shown in Fig. 2 (a). The grating is fabricated at Institute of Microelectronics (IME), Singapore. The detailed fabrication process can be referred to [18]. The top-view microscope image is taken and shown as Fig. 2 (b). The focusing structure is used to shrink the device footprint.

We characterize the grating coupler by measuring the insertion loss of a pair of input/output grating coupler which is connected by a short waveguide that we assume is lossless. The tunable laser (NPI Super Tune-2000) continuous wave output went through the polarization controller made by SM-1950 jump fiber. At the output of the chip, we measure the optical power by an InGaAs power meter from Thorlabs (S148C). We scan the laser in a step mode with 5 nm resolution from 1935 nm to 1980 nm. The measured peak efficiency is $-$8.4 dB at 1950 nm as we designed. The coupling efficiency curve is normalized and plotted in Fig. 2 (a). The discrepancy between the simulated and the measured coupling efficiency is due to the limited UV lithography resolution for those narrow grating lines (<200 nm). This problem should be avoided by redesigning the fill factor and period to make sure the minimum gap is large enough.

III. Waveguide Bend

The waveguide bend suffers from more radiation leakage at 2-μm than at 1.5-μm. Here we theoretically and experimentally investigate the bending loss for both strip and rib waveguide at 1950 nm. It is a trade-off to design the waveguide width since large width reduces the impact from sidewall roughness while it induces larger radiation loss. We calculate the maximum waveguide widths allowed for the single quasi-TE mode from wavelength of 1450 nm to 2050 nm by finite element method (FEM) as shown in Fig. 3. Based on a balanced consideration between the radiation loss and the side wall scattering loss, we select a waveguide width of 600 nm at 1950 nm for both strip and rib waveguides. The cross section geometry of the deeply etched strip waveguide and the rib waveguide with 90 nm slab are shown in Fig. 4. The corresponding quasi-TE mode field distributions are calculated and are shown in Fig. 4 (a), (b).

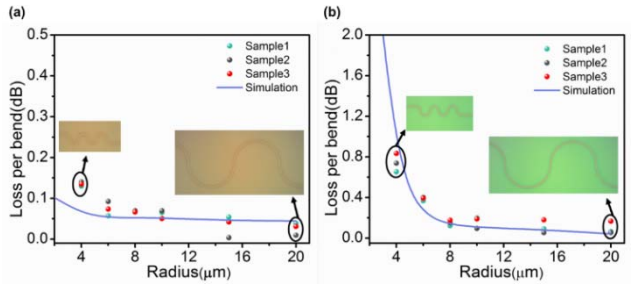

Fig. 5. (a) The simulated and the measured bending loss for strip waveguides. (b) The simulated and the measured bending loss for rib waveguides with 130 nm etching depth. Inset: the microscope images of the bends with radius of 4 μm and 20 μm.

The rib waveguide is shallow etched with 130 nm etching depth. The fabrication process is the same with the grating coupler. For both strip and rib waveguide, the bending losses are calculated by measuring a series of long waveguides with different number of bends. The microscope images of the bent waveguide with radius of 20 μm and 4 μm are shown in the inset of Fig. 5 with the same scale. The different color reveals that the etching depth is different for the two waveguides. The measured strip waveguide bending losses with bending radius from 4 μm to 20 μm are plotted as scatter points in Fig. 5. (a). We measured the bending losses from three dies which are not adjacent to each other in the wafer. We can see that the performance variations are small between different dies. The bending loss increases significantly when the radius is smaller than 8 μm. The average bending loss for radius of 20 μm is 0.026 dB / bend. The theoretical losses are calculated by 3D FDTD simulations and are plotted in Fig. 5 (a) as a solid curve. The experimental data is consistent with the theoretical predictions except for the bends with radius of 4 μm. For the rib waveguide, the experimental data matches well with the simulation results. The bending losses are larger than that of the strip waveguide due to the weaker mode confinement. The average bending loss for radius of 20 μm is 0.095 dB / bend. Similar to the strip waveguide, the bending radius has to be larger than 8 μm to maintain a low loss. From the above measured results and the theoretical predictions, we expect that 600 nm-wide waveguide can be used for single mode waveguide at both 1.55-μm and 2-μm. A low bending loss can be achieved when the bending radius is above 8 μm.

IV. Tunable Microring

The add drop microring resonator is a highly functional device for many applications [19]–[26]. The microring is designed as a race track structure. The bending radius, coupling length, coupling gap distance is 10 μm, 12 μm, 200 nm, respectively. The waveguide layer is fabricated using the same process as the grating coupler and the waveguide bend. An additional layer of titanium nitride is used as the heater to make the ring tunable. The heater is on top of the ring waveguide and is contacted with the metal pad through contact via. The microscope image of the tunable ring is shown in Fig. 6. We measure the ring spectral characteristics by

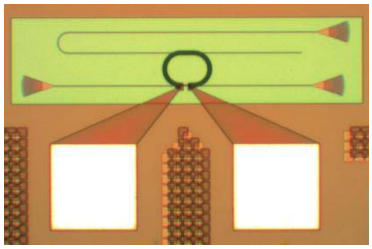

Fig. 6. The top-view microscope image of the tunable microring resonator.

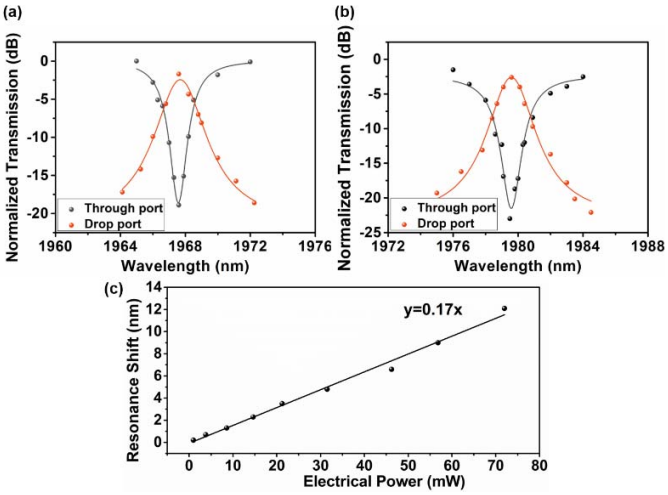

Fig. 7. The measured ring resonances of both through port and drop port at (a) 1967.6 nm and (b) 1979.5 nm. (c) The measured resonance shift as a function of the consumed electrical power.

using the tunable laser and the power meter that operate at two micrometer band. The ring resonance of both through port and drop port is recorded as shown in Fig. 7. (a) and (b) which corresponds to two adjacent resonances located at 1967.6 nm and 1979.5 nm. The free spectral range is $\sim$ 12 nm. The extinction ratio exceeds 20 dB for both two resonances. The highest quality factor measured at the through port ($\lambda = 1967.6$ nm) is 1520.

The microring can be implemented as either notch filter or band pass filter at the resonant wavelength [20]. Higher quality factor can be achieved by changing the coupling condition at the coupling region. Another property that required for a filter is the wavelength tuning. The doped silicon can be used as resistive layer to generate heat but it induces excess loss. Here we use a TiN layer to heat up the ring and hence change the refractive index of the ring waveguide. The electrical current is injected onto the resistor to generate the heat. We plot the resonance shift as a function of the applied electrical power, as shown in Fig. 7 (c). The resonance shift increases linearly with the applied electrical power. The thermal tuning efficiency is $\sim$0.17 nm/mW.

V. Conclusion

In summary, we have designed, fabricated, and characterized the grating coupler, waveguide bends and wavelength tunable add-drop microring resonator at 2-μm. The components

are fabricated by the same MPW process and on the same silicon-on-insulator substrate with the 1.5-μm devices. The grating coupler can couple the TE polarized light into the SM-1950 fiber with -8.4 dB efficiency. The strip waveguide and rib waveguide bending losses are measured and the results are consistent with the FDTD simulations. Finally we have demonstrated an add-drop microring resonator with a quality factor of 1520 at 1967.6 nm. The microring can be thermally tuned with efficiency of 0.17 nm / mW. The silicon photonics at 2-μm band will be beneficial for on-chip optical interconnect, sensing, spectroscopy and many other applications.

ACKNOWLEDGEMENT

The authors thank IME Singapore for the device fabrication and NPI LASERS for providing the laser.

REFERENCES

[1] P. Werle, F. Slemr, K. Maurer, R. Kormann, R. Mucke, and B. Janker, "Near- and mid-infrared laser-optical sensors for gas analysis," *Opt. Lasers Eng.*, vol. 37, nos. 2–3, pp. 101–114, 2002.

[2] Z. Liu *et al.*, "Up to 64QAM (30 Gbit/s) directly-modulated and directly-detected OFDM at 2 μm wavelength," in *Proc. ECOC*, Cannes, France, Nov. 2014, pp. 1–3, paper Tu.4.3.5.

[3] A. M. Heidt, Z. Li, and D. J. Richardson, "High power diode-seeded fiber amplifiers at 2 μm—From architectures to applications," *IEEE J. Sel. Topics Quantum Electron.*, vol. 20, no. 5, Mar. 2014, Art. no. 3100612.

[4] M. A. Van Camp *et al.*, "Demonstration of electrooptic modulation at 2165 nm using a silicon Mach–Zehnder interferometer," *Opt. Exp.*, vol. 20, no. 27, pp. 28009–28016, 2012.

[5] Y. Dong *et al.*, "Two-micron-wavelength germanium-tin photodiodes with low dark current and gigahertz bandwidth," *Opt. Exp.*, vol. 25, no. 14, pp. 15818–15827, 2017.

[6] Y.-H. Peng, H. H. Chang, V. L. Mashanov, and G.-E. Chang, "GeSn *p-i-n* waveguie photodetectors on silicon substrates," *Appl. Phys. Lett.*, vol. 105, no. 23, pp. 1109–1114, Nov. 2014.

[7] M. N. Petrovich *et al.*, "First demonstration of 2 μm data transmission in a low-loss hollow core photonic bandgap fiber," *Opt. Exp.*, vol. 21, no. 13, pp. 28559–28569, Sep. 2012.

[8] Z. Liu *et al.*, "52.6 Gbit/s single-channel directly-modulated optical transmitter for 2-μm spectral region," in *Proc. Opt. Fiber Commun. Conf.*, Mar. 2015, paper Th1E.6.

[9] K. Xu, L. Sun, Y. Xie, Q. Song, J. Du, and Z. He, "Transmission of IM/DD signals at 2 μm wavelength using PAM and CAP," *IEEE Photon. J.*, vol. 8, no. 5, Oct. 2016, Art. no. 7906407.

[10] H. Zhang *et al.*, "100 Gbit/s WDM transmission at 2 μm: Transmission studies in both low-loss hollow core photonic bandgap fiber and solid core fiber," *Opt. Exp.*, vol. 23, no. 4, pp. 4946–4951, 2015.

[11] K. Xu, Q. Wu, Y. Xie, M. Tang, S. Fu, and D. Liu, "High speed single-wavelength modulation and transmission at 2 μm under bandwidth-constrained condition," *Opt. Exp.*, vol. 25, no. 4, pp. 4528–4534, 2017.

[12] G. Roelkens *et al.*, "Silicon-based photonic integration beyond the telecommunication wavelength range," *IEEE J. Sel. Topics Quantum Electron.*, vol. 20, no. 4, Jul./Aug. 2014, Art. no. 8201511.

[13] H. Zhang *et al.*, "Dense WDM transmission at 2 μm enabled by an arrayed waveguide grating," *Opt. Lett.*, vol. 40, no. 14, pp. 3308–3311, 2015.

[14] N. Ye *et al.*, "Demonstration of 90° optical hybrid at 2 μm wavelength range based on 4×4 MMI using diluted waveguide," in *Proc. ECOC*, Cannes, France, Nov. 2014, pp. 1–3, paper P.2.14.

[15] J. J. Ackert *et al.*, "High-speed detection at two micrometres with monolithic silicon photodiodes," *Nature Photon.*, vol. 9, no. 10, pp. 393–396, May 2015.

[16] R. Wang *et al.*, "2 μm wavelength range InP-based type-II quantum well photodiodes heterogeneously integrated on silicon photonic integrated circuits," *Opt. Exp.*, vol. 23, no. 20, pp. 26834–26841, 2015.

[17] M. S. Rouifed *et al.*, "Ultra-compact MMI-based beam splitter demultiplexer for the NIR/MIR wavelengths of 1.55 μm and 2 μm," *Opt. Exp.*, vol. 25, no. 10, pp. 10893–10900, 2017.

[18] K. Xu, G. K. P. Lei, S. M. G. Lo, Z. Cheng, C. Shu, and H. K. Tsang, "Bit-rate-variable DPSK demodulation using silicon microring resonators with electro-optic wavelength tuning," *IEEE Photon. Technol. Lett.*, vol. 24, no. 14, pp. 1221–1223, Jul. 15, 2012.

[19] X. Wu, C. Huang, K. Xu, C. Shu, and H. K. Tsang, "128-Gb/s line rate OFDM signal modulation using an integrated silicon microring modulator," *IEEE Photon. Technol. Lett.*, vol. 28, no. 19, pp. 2508–2561, Oct. 1, 2016.

[20] C. W. Chow, C. H. Yeh, S. M. G. Lo, C. Li, and H. K. Tsang, "Long-reach radio-over-fiber signal distribution using single-sideband signal generated by a silicon-modulator," *Opt. Exp.*, vol. 19, no. 12, pp. 11312–11317, Jun. 2011.

[21] K. Xu *et al.*, "Amplitude and phase modulation of UWB monocycle pulses on a silicon photonic chip," *IEEE Photon. Technol. Lett.*, vol. 28, no. 3, pp. 248–251, Feb. 1, 2016.

[22] F. Xia, L. Sekaric, and Y. Vlasov, "Ultracompact optical buffers on a silicon chip," *Nature Photon.*, vol. 1, no. 1, pp. 65–71, 2007.

[23] F. Liu *et al.*, "Compact optical temporal differentiator based on silicon microring resonator," *Opt. Exp.*, vol. 16, no. 20, pp. 15880–15886, 2008.

[24] D. Dai, "Highly sensitive digital optical sensor based on cascaded high-Q ring resonators," *Opt. Exp.*, vol. 17, no. 26, pp. 23817–23822, 2009.

[25] A. C. Turner, M. A. Foster, A. L. Gaeta, and M. Lipson, "Ultra-low power parametric frequency conversion in a silicon microring resonator," *Opt. Exp.*, vol. 16, no. 7, pp. 4881–4887, 2008.

[26] R. Kumar, M. Savanier, J. Ong, and S. Mookherjea, "Entanglement measurement of a coupled silicon microring photon pair source," *Opt. Exp.*, vol. 23, no. 15, pp. 19318–19327, 2015.